PAPER VII

Analysis of the time-averaged gas–solid drag force based on data from transient 3D CFD simulations of fluidized beds

Powder Technology 274 (2015) 227–238.
Copyright 2015 Elsevier B.V.
Reprinted with permission from the publisher.

Powder Technology 274 (2015) 227–238

Contents lists available at ScienceDirect

Powder Technology

journal homepage: www.elsevier.com/locate/powtec

Analysis of the time-averaged gas–solid drag force based on data from transient 3D CFD simulations of fluidized beds

Sirpa Kallio *, Juho Peltola, Timo Niemi

VTT Technical Research Centre of Finland, P.O. Box 1000, FI-02044 VTT, Finland

ARTICLE INFO

Article history:
Received 6 August 2014
Received in revised form 8 January 2015
Accepted 10 January 2015
Available online 15 January 2015

Keywords:
Drag force
Fluidized bed
Time-averaged
3D

ABSTRACT

In the present work, a qualitative analysis of the time-averaged gas–solid drag force in gas–solid fluidized beds is carried out. The analysis is based on a large number of transient Eulerian–Eulerian 3D CFD simulations of small bubbling, turbulent and circulating fluidized beds. The obtained results significantly differ from corresponding data previously obtained from 2D simulations, especially at high solid concentrations. This confirms that to accurately model the gas–solid drag force in a steady state 3D simulation, the drag model should not be based on data from transient 2D simulations. In the present work, the average drag force is expressed as the product of the drag force calculated from time-averaged velocities and volume fractions and a correction coefficient. The study shows that even when the third dimension is described in the mesh with only three nodes, the 3D character of the flow is captured in the drag correction coefficient. Thus, a large number of parametric studies could be carried out in a reasonable time frame. In the paper, the parameters affecting the time-averaged drag force are identified and the nature of the effects are analyzed. The analysis shows that solid volume fraction, particle size, solid density, gas viscosity, the slip velocity between gas and solids and the lateral distance to a wall have significant effects on the drag correction coefficient. At high gas densities typical e.g. of pressurized fluidization even the gas density has significant effects. A closure relation for the time-averaged drag force for a wide range of fluidization conditions should include these seven variables as inputs.

© 2015 Elsevier B.V. All rights reserved.

1. Introduction

Computational fluid dynamics (CFD) has in the past decades become a popular and efficient tool for process design. In case of multiphase processes the development has been slower than for single phase processes due to theoretical complications related to phase interactions and the greater requirements for computational capacity. Large size of industrial facilities further complicates application of multiphase CFD. Fluidized beds are no exception and only recently simulation of large industrial fluidized beds has become feasible. However, computation times in simulations with the most accurate models are still too long and hence modifications and adaptations to the modeling approaches are needed to apply them in commercial scale.

Characteristic of dense gas–solid flow is the occurrence of inhomogeneous structures like clusters and strands of particles in circulating fluidized bed (CFB) conditions and bubbles and voids in bubbling (BFB) and turbulent fluidized beds (TFB). Fluidized beds are commonly simulated in the transient mode in which the transient inhomogeneous flow patterns should ideally be resolved by the simulation. Such approach would require a fine spatial and temporal resolution which leads to a computation time that would be orders of magnitude too long in industrial applications. A solution to the problem is to decrease the resolution and include closure models that describe the effects of the unresolved sub-grid scale structures [1–3]. Largest emphasis in the development of sub-grid scale closures has so far been on the gas–solid drag force which is commonly expressed as a product of the drag force calculated from the correlations for homogeneous suspensions and a correction factor that is a function of the mesh spacing, suspension density and other parameters characterizing the flow structure such as the distance to the wall and gas-solid slip velocity [4].

As an alternative to the transient coarse mesh simulation approach, models for steady-state simulation have been developed by time-averaging the transient fluid flow equations [5,6]. The obvious benefit of this approach is that the time-consuming integration of the transient simulation results, which needs to be done to analyze average conditions in the process, is avoided. The required closure laws are similar to the closure laws needed for transient coarse mesh simulations with the difference that the closure laws for time-averaged equations are not dependent on the mesh spacing to equal extent, which simplifies modeling [7]. In a situation where the filter scale of a transient simulation is significantly larger than the inhomogeneous flow structures, the transient and time-averaged closure models are one and the same.

One of the largest terms in the time-averaged momentum equations is the gas–solid drag force. Similar to the sub-grid drag closures, the closure law for time-averaged drag can be written by means of a correction function applied on the drag force calculated assuming homogeneous conditions. In the study of Taivassalo et al. [5], correction functions

* Corresponding author. Tel.: +358 20 7224015.
E-mail address: sirpa.kallio@vtt.fi (S. Kallio).

http://dx.doi.org/10.1016/j.powtec.2015.01.029
0032-5910/© 2015 Elsevier B.V. All rights reserved.

Notation

C_d	drag coefficient
d	diameter
D	depth of the bed
H	height of the riser
K_{gs}	inter-phase momentum transfer coefficient
Re	Reynolds number
u	velocity
U	time-averaged velocity
U_0	superficial velocity
v_t	terminal velocity
W	riser width
x	distance
Δx_{mesh}	mesh spacing
$\Delta x_{H,W}$	mesh spacing along width and height
Δx_D	mesh spacing in depth direction
Δx_{wall}	distance to a wall
$\Delta x_{f\ \&b}$	distance to the front wall or the back wall (minimum of the two)

Greek symbols

α	volume fraction
μ	viscosity
ρ	density

Subscripts

Ergun	Ergun drag law
g	gas
gs	gas–solid interaction
p	particle
s	solid
t	related to terminal velocity
W–Y	Wen & Yu drag law

Superscripts

*	calculated from time-averaged values

developed on the basis of transient 2D simulation data were applied. In these simple closure laws the correction was expressed as a function of solid volume fraction. Kallio et al. [8] analyzed drag data from a large number 2D simulations of CFBs to evaluate the properties that can affect the average drag force. Altogether six variables, i.e. solid volume fraction, slip velocity, distance to the wall, solid material density, particle size and gas viscosity were listed as potential input variables for a drag correction correlation, which indicates that the models used in [5] could be too simple to cover the wide range of conditions encountered in a fluidized bed. The results in the study of Kallio et al. [7] showed that on the basis of drag data collected from transient

Table 1
The models and parameters used in the simulations.

Submodel or parameter	Model or value used
Granular viscosity	Syamlal et al. [12]
Granular bulk viscosity	Lun et al. [13]
Frictional viscosity	Schaeffer [14]
Granular conductivity	Syamlal et al. [12]
Solids pressure	Lun et al. [13]
Radial distribution	Ogawa et al. [15]
Angle of internal friction	30°
Frictional and packing limit	0.61 and 0.63, respectively
Turbulence model	Standard k-ε, dispersed
Wall boundary condition, gas phase	No slip
Wall boundary condition, solid phase	Partial slip, specularity coefficient 0.001

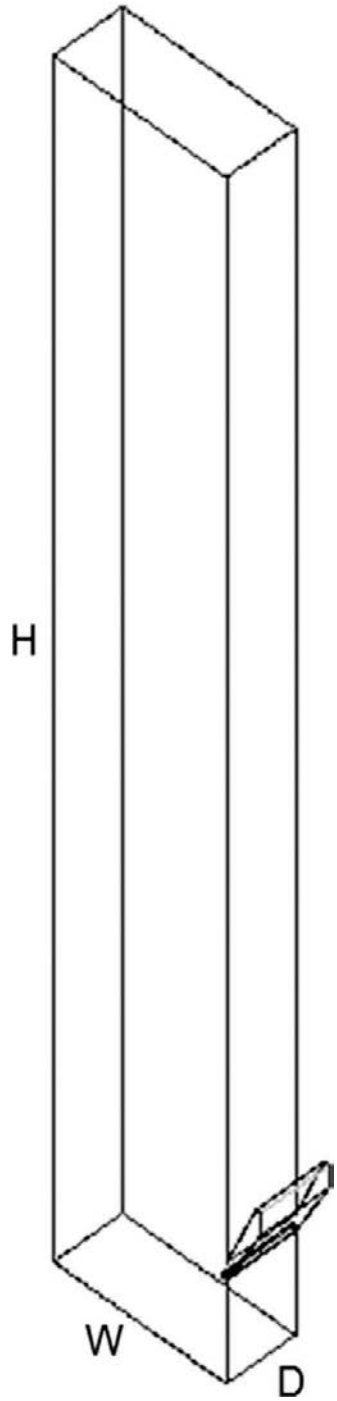

Fig. 1. The geometry of a simulated fluidized bed with depth D, width W and height H.

simulations it is possible to derive correlations that can be used in time-averaged simulations. In addition to the six parameters suggested in the study of Kallio et al. [8], height above air distributor and local gas superficial velocity were used as input parameters. The work was based on 2D simulation data covering both BFB and CFB conditions. Several comparisons of 2D and 3D CFD simulation results have been carried out in the literature [9,10]. The reported significant effects of the dimensionality imply that utilization of 2D simulation data can reduce the accuracy of the developed correlations, when they are applied in 3D simulations.

In the present paper, data from transient 3D simulations are analyzed and the results are compared with the earlier ones [7,8] obtained from 2D simulations. Like in the previous work, the present study is limited to Geldart B particles and the analysis is done only for the vertical drag force component. Due to the long simulation times of transient 3D cases, only a very limited amount of data is to date available and mainly from small fluidized beds. In the paper, the quality of the 3D simulations and the produced data is discussed. The amount of data is sufficient for the present qualitative study that presents a survey of the possibility to define the variables for an intended development of a general closure model for the drag force in fluidized bed conditions. However, more data should be included in the future if the data are to be used as the basis for development of such a general drag correlation.

2. Transient Eulerian–Eulerian 3D simulations

2.1. Methods used

The same models and numerical methods as used in the 2D studies of Kallio et al. [7,8] were used here in the 3D simulations. The simulations were carried out with the commercial code ANSYS Fluent v.14 [11] with the Eulerian–Eulerian multiphase approach based on the kinetic theory of granular flow (KTGF). The models used are listed in Table 1 and they are given in detail in the study of Kallio et al. [7].

As in the previous 2D study, the drag term was computed from the Gidaspow [16] drag model, which combines the Ergun [17] and Wen–Yu [18] drag laws. A second order discretization scheme was used for momentum and the QUICK scheme for the volume fraction equation. The time step was 0.001 s for the 10 mm and coarser meshes and 0.0005 s for the 6.25 mm and finer meshes. To validate the modeling approach, comparisons with measurements have earlier been carried out for some 2D simulations with the same models in a 0.4 m wide geometry [19]. The measurement and simulation results were in good qualitative agreement and even quantitatively the results were acceptable. On that basis the chosen approach can be considered sufficiently accurate for the present study. For each case, approximately 5 s was simulated before starting time-averaging. A further 120 s of flow time was simulated to compute the averages, which guarantees a sufficient accuracy.

2.2. The simulated cases

The 2D geometry in the study of Kallio et al.[7,8] was a simple riser with straight walls. In the present study, a similar 3D geometry, shown in Fig. 1, is used. Two alternative descriptions for air distribution were applied: a uniform gas inflow rate at riser bottom and a non-uniform distribution in which air enters through orifices placed about 5 cm apart from each other. Solids left the riser through the top edge of the simulated domain and were fed back through a return channel, the opening of which was located at 0.6–0.7 m height in the riser.

Kallio et al. [7,8] observed that simulations with mesh spacing 12 mm gave the same result for the correction coefficient for the time-averaged drag force as simulations in a finer mesh with 6 mm elements. To save computation time, most of the simulations in the present study

Table 2
Simulated cases. Inlet types marked with texts 'unif.' for uniform gas distribution and 'orif.' for air distributed through separate orifices at riser bottom.

	Inlet type	U_0	μ_g	ρ_g	ρ_s	d_p	$\Delta_{H,W}$	Δ_D	W	H	D	Average α_s	v_t	Ar	U_0/v_t
		m/s	kg/ms	kg/m^3	kg/m^3	mm	mm	mm	m	m	m	–	m/s	–	–
1	unif.	5	4.45E-5	0.3105	2480	0.255	13.3	13.3	1	7	0.4	0.0297	1.53	63.2	3.27
2	unif.	2.75	4.45E-5	0.3105	2480	0.6	12.5	12.5	0.4	3	0.0375	0.0270	4.96	824	0.55
3	unif.	0.6	4.45E-5	0.3105	2480	0.15	12.5	12.5	0.4	3	0.0375	0.0270	0.62	12.9	0.97
4	unif.	1.3	4.45E-5	0.3105	2480	0.15	12.5	12.5	0.4	3	0.0375	0.0270	0.62	12.9	2.10
5	unif.	2.75	4.45E-5	0.3105	2480	0.255	12.5	12.5	0.4	3	0.0375	0.0270	1.53	63.2	1.80
6	unif.	2.75	4.45E-5	0.3105	2480	0.255	6.25	6.25	0.4	3	0.0375	0.0270	1.53	63.2	1.80
7	unif.	1.3	4.45E-5	1.255	2480	0.255	12.5	12.5	0.4	3	0.0375	0.0269	1.20	255	1.08
8	unif.	2.75	4.45E-5	1.255	2480	0.255	12.5	12.5	0.4	3	0.0375	0.0268	1.20	255	2.30
9	unif.	2.75	1.79E-5	0.3105	2480	0.255	12.5	12.5	0.4	3	0.0375	0.0270	2.70	391	1.02
10	unif.	2.75	1.79E-5	0.3105	2480	0.255	12.5	12.5	0.4	3	0.1125	0.0269	2.70	391	1.02
11	unif.	2.75	4.45E-5	6	2480	0.255	12.5	12.5	0.4	3	0.0375	0.0267	0.81	1219	3.40
12	unif.	2.75	3.00E-5	0.3105	2480	0.255	12.5	12.5	0.4	3	0.0375	0.0270	1.99	139	1.38
13	unif.	1.3	4.45E-5	1.255	2480	0.15	12.5	12.5	0.4	3	0.0375	0.0268	0.54	52.0	2.41
14	unif.	1.3	4.45E-5	1.255	1500	0.255	12.5	12.5	0.4	3	0.0375	0.0268	0.80	155	1.63
15	orif.	1	4.45E-5	0.311	2480	0.255	10	5	0.4	3	0.015	0.0660	1.53	63.3	0.65
16	orif.	5	4.45E-5	0.311	2480	0.44	10	5	0.4	3	0.015	0.0660	3.37	325	1.48
17	orif.	2	4.45E-5	0.311	2480	0.255	10	5	0.4	3	0.015	0.0660	1.53	63.3	1.31
18	orif.	1.6	4.45E-5	0.311	2480	0.255	10	5	0.4	3	0.015	0.0660	1.53	63.3	1.05
19	orif.	1.3	4.45E-5	0.311	2480	0.255	10	5	0.4	3	0.015	0.0660	1.53	63.3	0.85
20	orif.	0.7	4.45E-5	0.311	2480	0.255	10	5	0.4	3	0.015	0.0660	1.53	63.3	0.46
21	orif.	0.5	4.45E-5	0.311	2480	0.255	10	5	0.4	3	0.015	0.0660	1.53	63.3	0.33
22	orif.	0.3	4.45E-5	0.311	2480	0.255	10	5	0.4	3	0.015	0.0660	1.53	63.3	0.20
23	unif.	1.25	1.79E-5	1.225	2480	0.255	12.5	12.5	0.4	3	0.0375	0.0666	1.86	1542	0.67
24	unif.	2.25	1.79E-5	1.225	2480	0.255	12.5	12.5	0.4	3	0.0375	0.3655	1.86	1542	1.21
25	unif.	2.75	1.79E-5	1.225	2480	0.255	12.5	12.5	0.4	3	0.0375	0.0391	1.86	1542	1.48
26	unif.	2.75	1.79E-5	1.225	2480	0.255	12.5	12.5	0.4	3	0.0375	0.0832	1.86	1542	1.48
27	orif.	1.25	1.79E-5	1.225	2480	0.255	10	5	0.4	3	0.015	0.0660	1.86	1542	0.67
28	orif.	2.25	1.79E-5	1.225	2480	0.255	10	5	0.4	3	0.015	0.0528	1.86	1542	1.21
29	orif.	2.75	1.79E-5	1.225	2480	0.255	10	5	0.4	3	0.015	0.0396	1.86	1542	1.48
30	orif.	2.75	1.79E-5	1.225	2480	0.255	5	5	0.4	3	0.015	0.0793	1.86	1542	1.48
31	orif.	2.75	1.79E-5	1.225	2480	0.255	10	5	0.4	3	0.015	0.0815	1.86	1542	1.48
32	unif.	2.5	4.45E-5	0.3105	2480	0.255	12.5	12.5	1	7	0.0375	0.0297	1.53	63.2	1.63

were carried out with a 12 mm mesh although in some runs a finer mesh was used to allow for grid sensitivity analysis. In case of 3D simulations, the computation time strongly limits the feasible mesh size. Thus, the third dimension was in the present study kept at the minimum to allow for a larger number of simulations. To analyze the effect of the small third dimension, an additional simulation with a significantly deeper bed was also carried out. In addition, simulations with varying number of elements in the third direction were done. The simulations cover the full range from bubbling to circulating fluidized bed conditions. Material property values and process conditions were varied to allow analysis of their effects. Their values were altered independently to reveal parametric effects. Thus, some of the simulated cases do not correspond to real conditions found in existing fluidized beds. In several cases, however, the gas is supposed to be air at room temperature or at around 850 °C, which is a typical CFB furnace temperature in boilers. Solid phase consists of spherical particles with restitution coefficient equal to 0.9. The simulations used as the basis for the present analysis are listed in Table 2. The average solids volume fractions given in the table are calculated from the time-averaged solids volume fraction obtained from each simulation by volume-averaging over the simulated geometry. The terminal particle velocity is estimated using the drag law of Haider & Levenspiel [20]. All the solid particles belong to the Geldart B group according to the original Geldart classification. However, if the effect of process parameters is taken into account, Cases 3, 4 and 13 are somewhat on the A-side of the A–B border [21]. Fig. 2 illustrates the solids distribution pattern obtained in Case 1, with distinct dense wall layers and a dense bottom bed.

Table 3
The transition function by Niemi et al. [20] which combines Ergun [17] and Wen–Yu [18] drag laws.

When $\alpha_g \geq 0.5$:

$$K_{gs} = K_{gs,W-Y} = \frac{3}{4} C_d \frac{\alpha_g \alpha_s \rho_g |\boldsymbol{u}_g - \boldsymbol{u}_s|}{d_p} a_g^{-2.65}$$

$$C_d = \begin{cases} \frac{24}{\mathrm{Re}}\left(1 + 0.15(\mathrm{Re})^{0.687}\right), & Re < 1000 \\ 0.44, & Re \geq 1000 \end{cases}$$

$$\mathrm{Re} = \frac{\alpha_g \rho_g |\boldsymbol{u}_g - \boldsymbol{u}_s| d_p}{\mu_g}$$

When $\alpha_g \leq 0.4$:

$$K_{gs} = K_{gs,Ergun} = 150 \frac{\alpha_s (1-\alpha_g)\mu_g}{\alpha_g d_p^2} + 1.75 \frac{\rho_g \alpha_s |\boldsymbol{u}_g - \boldsymbol{u}_s|}{d_p}$$

When $0.4 < \alpha_g < 0.5$:

$$K_{gs} = K_{gs,Ergun} + 10(\alpha_g - 0.4)(K_{gs,W-Y} - K_{gs,Ergun})$$

2.3. Time-averaging

As in the study of Kallio et al. [8], the transient data from each simulation were time-averaged to determine in each mesh point the average flow properties and the average drag force. As in the previous 2D study

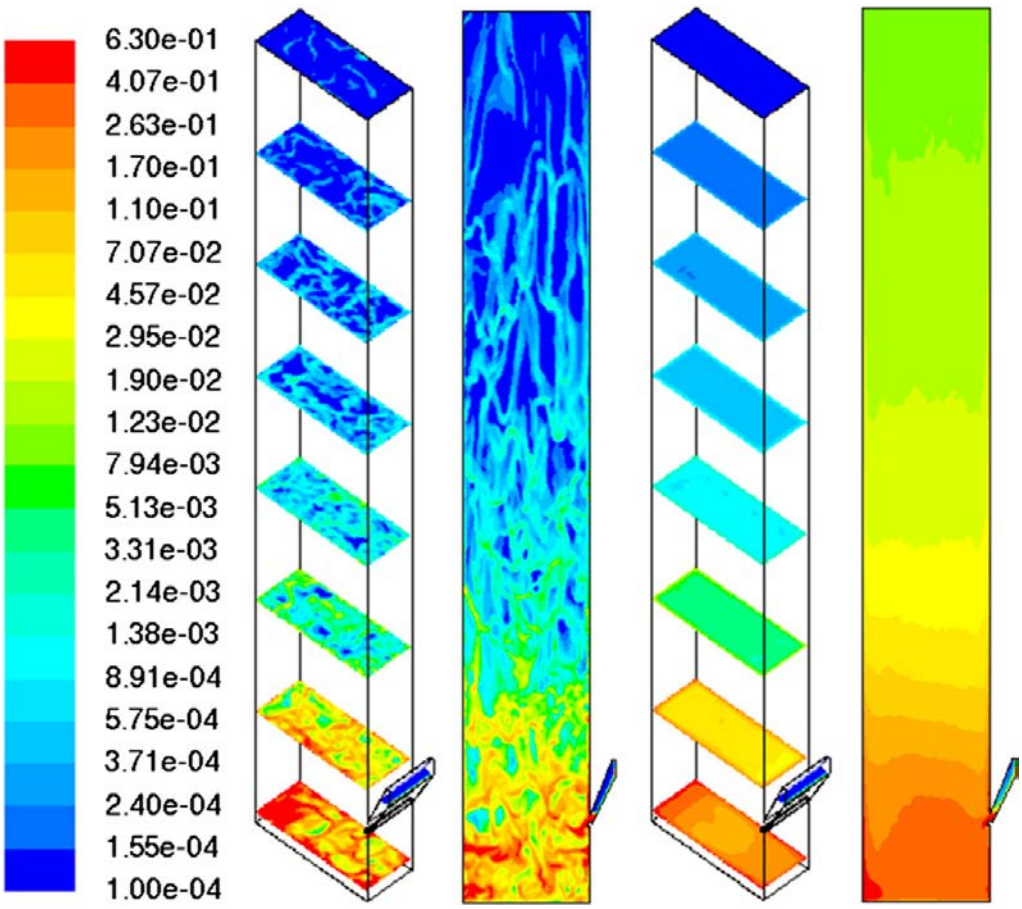

Fig. 2. Transient (left) and time-averaged (right) distribution of solid volume fraction at eight elevations and on the middle plane of the riser.

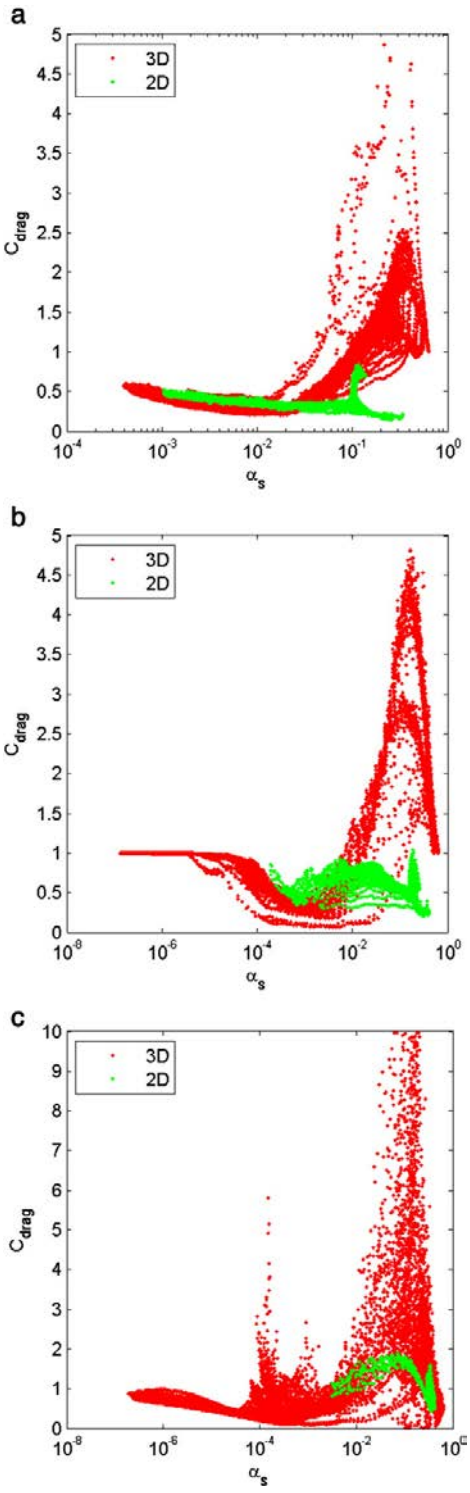

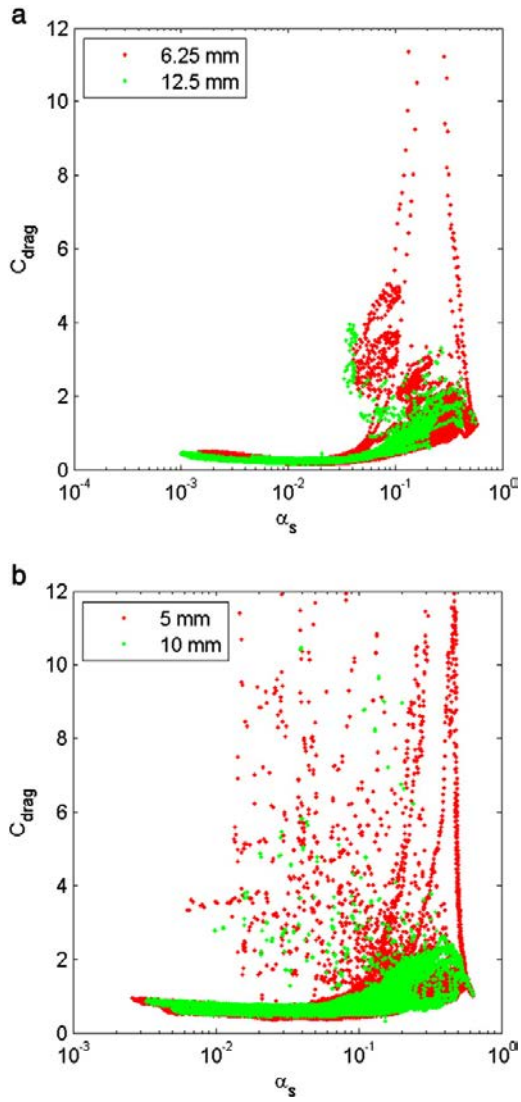

Fig. 4. Effect of mesh resolution a) in Cases 6 and 5 (mesh resolution was the same in all directions, $\mu_g = 4.45e{-}5$ kg/ms, $\rho_g = 0.311$ kg/m^3, $\rho_s = 2480$ kg/m^3, $d_p = 0.255$ mm. $U_0 = 2.75$ m/s), and b) in Cases 30 and 31, (mesh resolution in the depth direction was 5 mm in both simulations while the resolution in the other directions was altered, $\mu_g = 1.79e{-}5$ kg/ms, $\rho_g = 1.225$ kg/m^3, $\rho_s = 2480$ kg/m^3, $d_p = 0.255$ mm. $U_0 = 2.75$ m/s).

[8], the analysis is done for the dominating vertical component of the drag force. The time-averaged drag force can be written in the form

$$\overline{K_{gs}\left(u_{g,y}-u_{s,y}\right)} = C_{drag}K^*_{gs}\left(U_{g,y}-U_{s,y}\right) \quad (1)$$

where $u_{g,y}$ and $u_{s,y}$ are the instantaneous gas and solid phase vertical velocity components and $U_{g,y}$ and $U_{s,y}$ the corresponding mass-weighted

Fig. 3. Comparison of C_{drag} determined from 3D simulation results with corresponding data from earlier 2D simulations [8]: a) CFB conditions (Case 17: $U_0 / v_t = 1.31$), b) TFB conditions (Case 15: $U_0 / v_t = 0.65$), and c) BFB conditions (Case 22: $U_0 / v_t = 0.20$). $\mu_g = 4.45e{-}5$ kg/ms, $\rho_g = 0.311$ kg/m^3, $\rho_s = 2480$ kg/m^3, $d_p = 0.255$ mm.

time-averaged velocity components. K_{gs}^{*} is the inter-phase momentum transfer coefficient calculated on the basis of the time-averaged velocities and volume fractions using a similar combination of Wen and Yu [18] and Ergun [17] drag laws as in the transient simulations. However, instead of using Gidaspow's [16] drag law, a smoother transition between the drag laws, suggested by Niemi et al. [22], was used to calculate K_{gs}^{*} (see Table 3). In this model a linear transformation over a range of solid volume fractions is done between the Ergun and Wen–Yu models. The coefficient C_{drag} in Eq. (1) is a drag correction coefficient. The value of C_{drag} in each point in the flow field can be calculated from Eq. (1) by time-averaging the drag force, solid volume fraction and gas and solid velocities over the simulation time of a transient simulation.

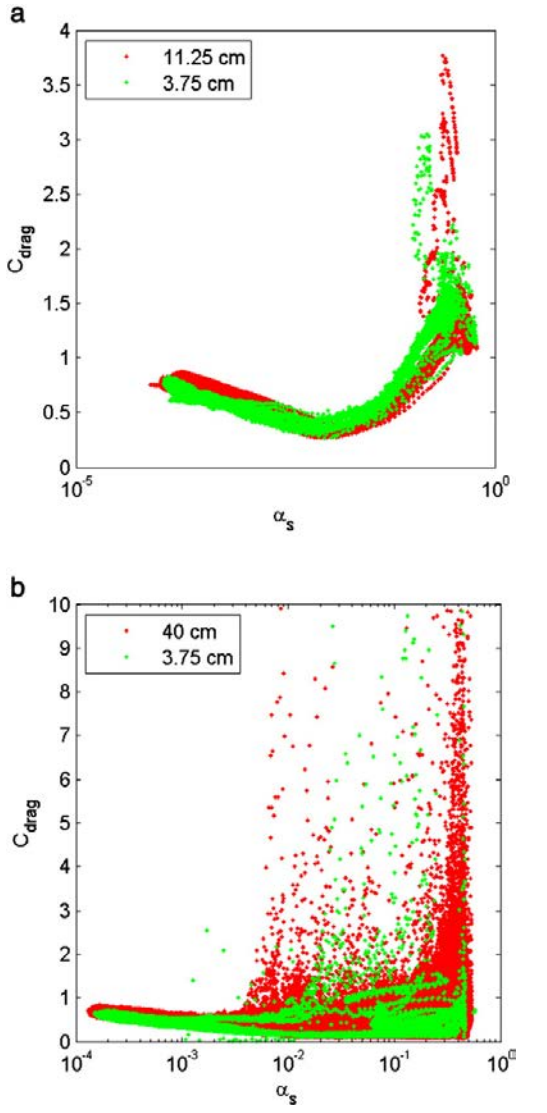

Fig. 5. Effect of the depth of the bed in different conditions: a) in Cases 10 and 9 (μ_g = 1.79e–5 kg/ms, ρ_s = 2480 kg/m^3, d_p = 0.255 mm, U_0 = 2.75 m/s, and b) in Cases 1 and 32 (μ_g = 4.45e–5 kg/m s, ρ_g = 0.311 kg/m^3, ρ_s = 2480 kg/m^3, d_p = 0.255 mm, U_0 = 5 m/s).

This kind of data was collected for each of the simulations. Filtering of the data was done at the data collection stage. For very low values of slip velocity, the computed C_{drag} can become unreasonably large or negative due to the stochastic nature of the data and the finite averaging periods. A minimum limit for the slip velocity magnitude was set at 0.001 m/s and all points with negative C_{drag} were excluded. The data for the solids return channel were also omitted at this stage from the analysis since the characteristics of the flow are there completely different. The uppermost half meter of the geometry was omitted to avoid possible exit effects.

3. Analysis of the results

3.1. Comparison with results of 2D simulations

It is fairly common to derive closure models for filtered momentum equations on the basis of results from transient 2D simulations [3,7]. However, how far the 2D results on the gas–solid drag force can be extended to 3D simulations needs to be assessed. For that purpose, several of the cases simulated in 2D in the study of Kallio et al. [7,8] were included in the present 3D analysis to allow direct comparison of the obtained C_{drag} values. Fig. 3 presents comparisons between 2D and 3D simulation results in CFB, TFB (turbulent fluidized bed) and BFB conditions. Since solid concentration is the most important variable affecting clustering and consequently also C_{drag}, the results are presented as a function of solid volume fraction α_s. Fig. 3 shows that the 2D simulations produced clearly different trends in BFB, TFB and CFB conditions. No similar significant difference between the fluidization modes can be seen in the 3D results and especially in the dense conditions of the CFB and TFB cases, the general trends in 2D and 3D results radically differ. Quantitatively, the C_{drag} values determined from 2D and 3D simulation data are similar in the dilute CFB conditions and also to some extent in BFB conditions, but in the dense bottom bed of a CFB and in a TFB the 2D results significantly deviate from the 3D results. In general, the 3D simulations produce higher C_{drag} at high solid concentrations. Thus a separate thorough 3D study of the gas–solid drag force, presented in this paper, is clearly necessary.

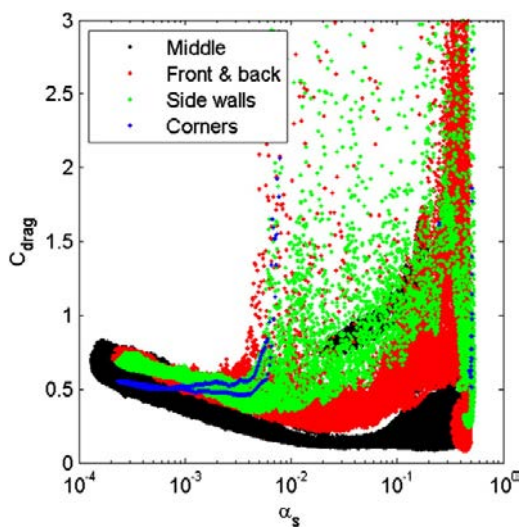

Fig. 6. C_{drag} in different geometrical regions in Case 1 (μ_g = 4.45e–5 kg/ms, ρ_g = 0.311 kg/m^3, ρ_s = 2480 kg/m^3, d_p = 0.255 mm, U_0 = 5 m/s).

3.2. Effect of mesh resolution and number of elements

To reduce computation time, the mesh resolution in the simulations of Table 2 was fairly coarse. Before analyzing effects of other parameters the possible effects of the mesh need to be evaluated. In the study of Kallio et al. [8], results obtained in 2D simulations with 25 mm, 12.5 mm and 6.25 mm mesh resolutions were compared. The two finest resolutions produced drag corrections of the same magnitude while the values obtained with the coarsest mesh were somewhat higher. A similar comparison was carried out in the 3D simulations of the present work. Fig. 4a illustrates the effect of the mesh in a simulation of a riser with a 0.4 m × 0.0375 m cross-section. With the coarser mesh, the depth direction is divided in three layers of computational elements while in the finer mesh the corresponding number of element layers is six. In the dense end of the solid concentration scale no large effect on C_{drag} can be observed. In dilute conditions the simulation with the coarser mesh produces lower C_{drag} values, which is contrary to what in general can be expected of a coarse mesh simulation. The larger number of elements in the depth direction in the finer mesh seems to reduce clustering resulting in slightly higher C_{drag}. Fig. 4b compares two simulations of a riser with 0.4 m × 0.015 m cross-section. In this mesh test, the mesh resolution was kept unchanged in the depth direction when the resolution in the other two directions was changed from 5 mm to 10 mm. No clear effect of the mesh can be observed in the bulk of the data other than an increase in the number of high C_{drag} values, especially at high α_s, which also was observed in Fig. 4a. These high values are a result of increased wall and corner effects in the finer mesh. In general we can conclude from Fig. 4 that a mesh resolution of 10–12.5 mm is sufficient to produce representative C_{drag} values. This conclusion is in agreement with the results from the earlier 2D studies [7,8]. Li et al. [23] showed that the required mesh resolution depends on the averaged variables that are considered in the analysis. Although flow structures smaller than 10–12 mm certainly exist in fluidized beds, their statistical significance for the average gas–solid drag force seems negligible which allows us to use fairly coarse mesh resolutions in the present study.

Computation time depends on the number of computational elements in the mesh. In addition to the mesh resolution, the selected geometry is also important. In the simulations analyzed in Fig. 4, the depth direction was small and the geometry corresponded to a pseudo-2D fluidized bed with a core-annular flow structure prevailing only in the width direction. Such geometries have been used in experiments to represent a 2D fluidized bed. Due to the relatively small number of cells that is required to describe a pseudo-2D fluidized bed, it would be beneficial for the present study, if the obtained C_{drag} would be representative of a 3D fluidized bed. To evaluate the applicability of this geometry, tests with different riser depths were carried out. Fig. 5 shows results from four such comparisons in different conditions. Although the results slightly change when riser depth is increased, the differences in all the two studied conditions are small. In Fig. 5b, where the differences in the depth and the number of mesh nodes in the depth direction are largest, there is clear difference in the results in the dense suspension region. This can be assumed to originate from the front and back

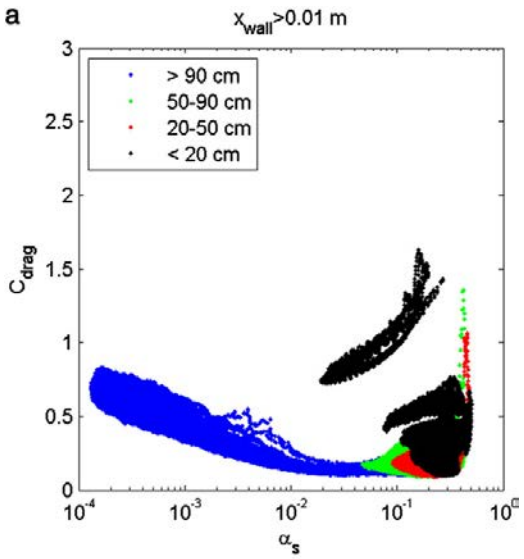

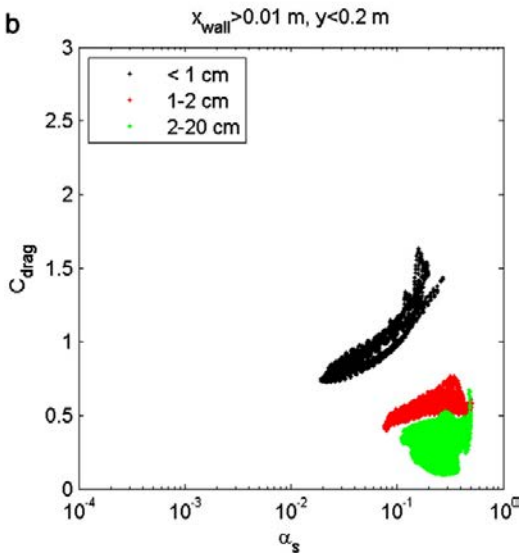

Fig. 7. C_{drag} in Case 1 in the middle section of the riser at different elevations.

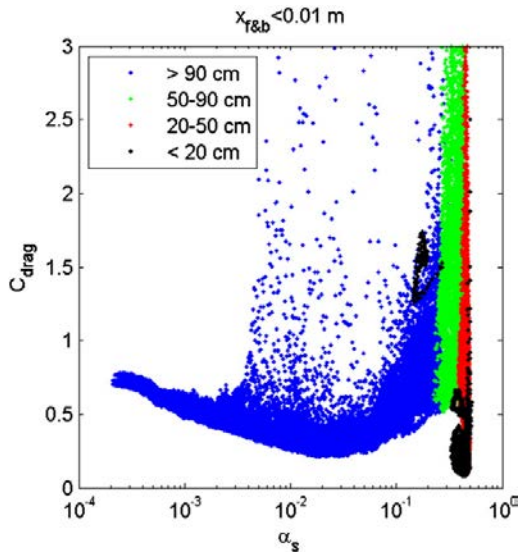

Fig. 8. C_{drag} in Case 1 in the vicinity of front and back walls at different elevations.

walls at which in the 0.4 m deep bed a dense down-flow-region is established. This is confirmed in the next section. In general, the effect of bed depth is relatively small which allows us to study parametric effects on the drag force by means of 3D simulations of pseudo-2D beds. Because of the shorter simulation time, it is thus feasible to carry out a larger number of simulations with wide variation in conditions in a reasonable time. Since the amount of data from dense suspension conditions increases with bed depth (see Fig. 5b), it would however be useful in the future to carry out more simulations in larger geometries to get a larger amount of data from conditions closer to the packing limit. Unfortunately, this could not be included in the present study. Still, enough data are available from the 32 simulations for the present qualitative analysis.

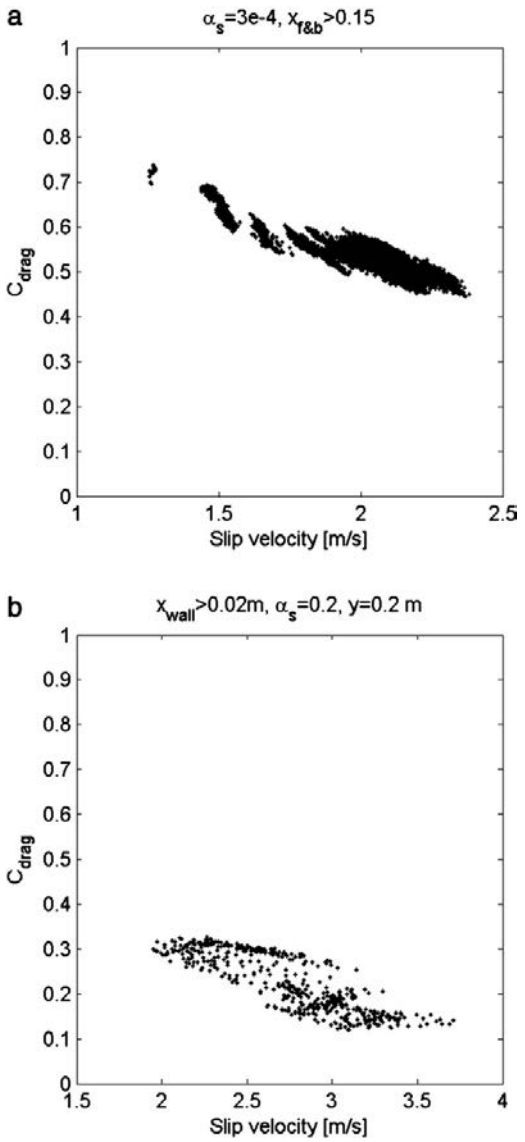

Fig. 9. Effect of slip velocity in the middle section of the riser in Case 1 a) in dilute conditions ($\alpha_s = 0.0003$) and b) at 0.2 m height in dense conditions ($\alpha_s = 0.2$).

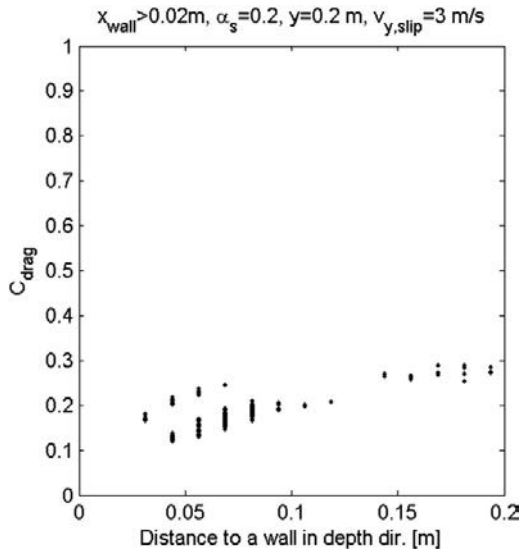

Fig. 10. Effect of the distance to a wall in the depth direction in the middle section of the riser at 0.2 m height in Case 1 when slip velocity is 3 m/s.

3.3. Regional effects

In dilute conditions, C_{drag} seems to be mainly a function of solid volume fraction if material properties are constant. In dense regions at solid volume fractions above 0.1%, there is a larger scatter in C_{drag} indicating that other variables than α_s have major effects. In earlier studies [3,4,8], the distance to the wall has been shown to be important. Of the simulations in Table 2, Case 1 with cross-section 1 m × 0.4 m offers best opportunities to evaluate the effects of the location in a fluidized bed on the drag correction coefficient.

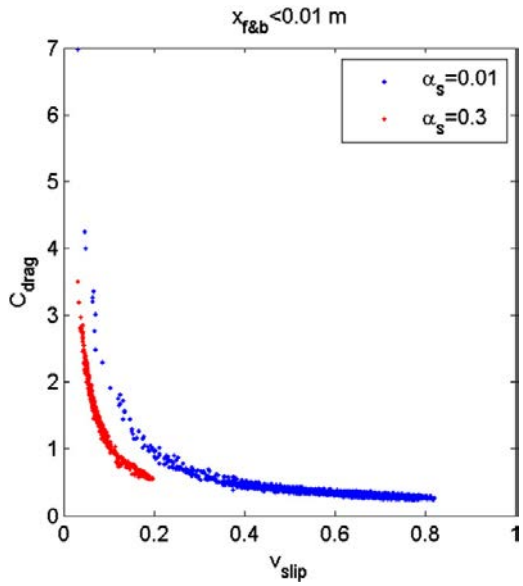

Fig. 11. Effect of slip velocity on C_{drag} at the front and back walls at solid volume fractions of 0.01 and 0.3.

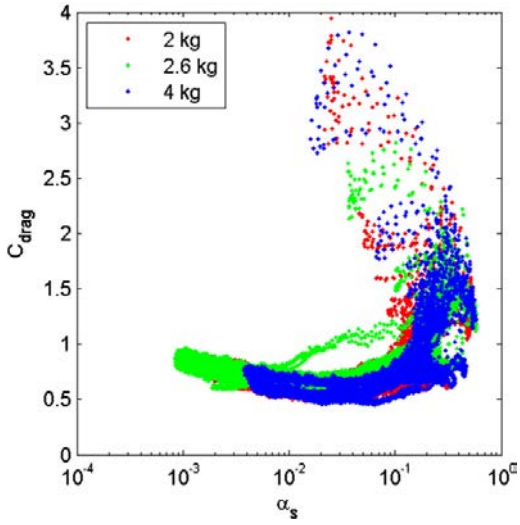

Fig. 12. Effect of solids inventory on C_{drag}. Cases 25, 24, and 26 in Table 2 ($\mu_g = 1.79e{-}5$ kg/ms, $\rho_g = 1.225$ kg/m^3, $\rho_s = 2480$ kg/m^3, $d_p = 0.255$ mm, $U_0 = 2.75$ m/s).

Fig. 6 shows C_{drag} in different regions of the CFB riser in Case 1. The riser is divided into four sections: front and back walls, side walls, corners and the middle section. Wall sections are defined as locations where the distance to the wall is below 10 mm while in the corners the distance to walls in both lateral directions is below the 10 mm limit. Close to walls, C_{drag} at solid volume fractions below 0.1 is systematically higher than in the middle region indicating that the suspension is more homogeneous close to a wall. The large scatter especially at high values of α_s needs to be analyzed further.

The data in the middle region of the riser are further split as a function of height in Fig. 7a. Fig. 7b shows that the two lower-most control volume layers at riser bottom produce clearly higher C_{drag} values than the rest of the riser volume. Both in the dilute and in the dense regions, there is a large scatter in C_{drag}, which indicates that other parameters than solid volume fraction significantly affect C_{drag}. A similar division as a function of height is presented in Fig. 8 for the wall layers at front and back walls. Significant scatter of values is also here present in the data and other parameters than α_s need to be considered.

3.4. Effect of the slip velocity and of the distance to a wall

Both slip velocity and the distance to a wall have been reported to affect the average drag force [4,8]. Fig. 9 illustrates the effect of the vertical slip velocity in dilute and dense conditions in the central region of a CFB riser. In both cases, increased slip velocity tends to reduce C_{drag}. Especially in the dense conditions, there remains a large scatter in the data even after the effects of solid volume fraction, slip velocity and elevation are removed. One possible parameter that can cause the scatter is the distance to the walls. Fig. 6 clearly showed that there is a clear difference between C_{drag} in the vicinity of a wall and C_{drag} in the central region. Whether there is an additional effect of the distance to the wall in the central region needs to be checked. Fig. 10 shows a clear effect of the distance to the front and back walls at slip velocity of 3 m/s. Interestingly, C_{drag} increases away from the wall, which means that there seems to be a minimum in C_{drag} close to the wall layer. At the wall, however, C_{drag} is according to Fig. 6. higher than in the central region.

At the wall, the slip velocity has a more pronounced effect than at riser center. Fig. 11 illustrates this effect at two solid volume fractions. The scatter in the values of C_{drag} at a specific solid volume fraction seems to be at the wall entirely caused by variations in the slip velocity. Similar to the central region in the riser, increased slip velocity reduces C_{drag}.

3.5. Effect of process conditions

Process conditions such as solids inventory, gas superficial velocity and air distributor design affect the flow patterns in a fluidized bed. They can also change the clustering tendency of the suspension and thus their effects on C_{drag} should be evaluated. Fig. 12 shows that the bed mass determines the range of solid volume fraction occurring in the fluidized bed but has no significant effect on C_{drag}. In dense conditions a small effect is visible. When bed mass increases, the location where a certain average solid volume fraction occurs will change. The differences seen in Fig. 12 at any specific value of solid volume fraction could thus, at least partly, be results of changed distance to a wall and to the air distributor.

Superficial gas velocity determines the state of fluidization for a given suspension. Fig. 13 shows the changes in C_{drag} as the gas velocity increases from 0.3 m/s to 2 m/s. At the lowest velocity the process is a BFB and at the highest velocity significant solids circulation takes place. No drastic change in the character of C_{drag} can be seen. At all velocities, reduction of the average drag force due to clustering takes place at low solid concentrations. Significant portion of the gas flow

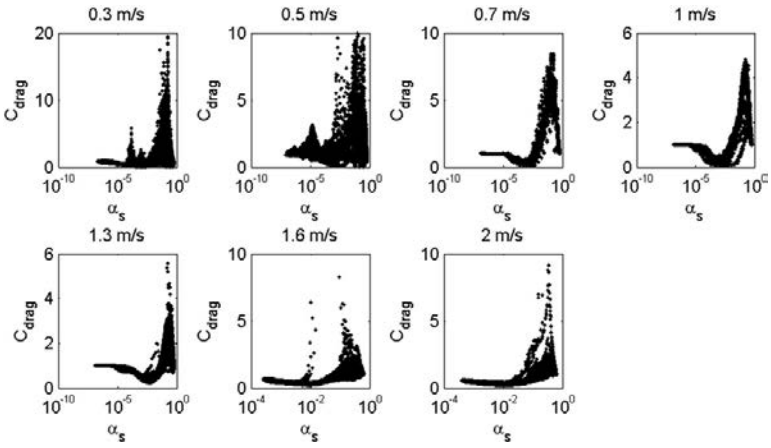

Fig. 13. Effect of superficial gas velocity on C_{drag} in Cases 17, 18, 19, 15, 20, 21, and 22, respectively ($\mu_g = 4.45e{-}5$ kg/ms, $\rho_g = 0.311$ kg/m^3, $\rho_s = 2480$ kg/m^3, $d_p = 0.255$ mm).

bypasses the clusters, which reduces the average drag force experienced by the particles. At very low solid volume fractions, C_{drag} is by definition equal to unity, which is also seen in the results. In the dense bottom and wall zones, an increase in C_{drag} above one is seen at all fluidization velocities. Although separation in dense and dilute suspension regions takes place even in the dense zones close to walls and at bed bottom, there the gas seems to travel more uniformly through both dense and dilute regions causing a significant drag force. Most particles in the bottom bed are located in the dense regions where the drag coefficient given by Ergun and Wen & Yu equations is high. Since the average drag force is by nature a volume-fraction-weighted property i.e. a Favre average, it is natural that C_{drag} can exceed unity in a dense suspension. At the packing limit the calculated values of C_{drag} are, in accordance with the definition of the drag correction coefficient, equal to unity.

Significant changes in the fluidization velocity affect the fluidization mode, which has great impact on the flow patterns and on the division of the suspension in dilute and dense suspension regions. Smaller changes in the fluidization velocity however do not affect the flow patterns in any significant way, especially in CFB conditions. Fig. 14 shows examples of effects of fluidization velocity in two cases. Even significant changes in fluidization velocities seem to be possible without any major change in C_{drag} in the dilute conditions. In the dense end of the scale the effects of the fluidization velocity are more pronounced. Fig. 14 b shows a case where the fluidization state changes from BFB to CFB as the fluidization velocity increases from 1.25 m/s to 2.75 m/s. This change is clearly visible in the results: in CFB conditions, the values of C_{drag} above unity occur at higher volume fractions than in BFB conditions.

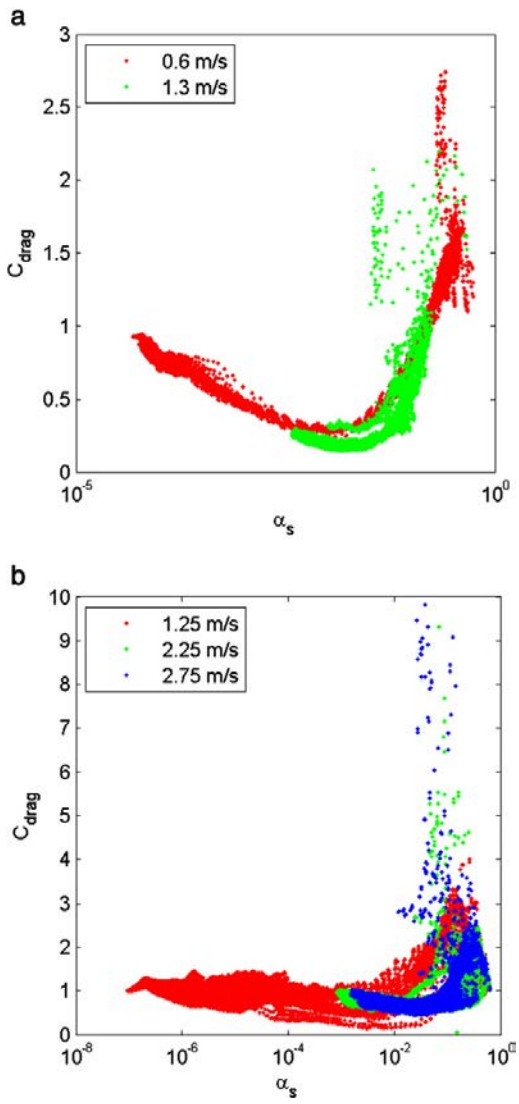

Fig. 14. Effect of fluidization velocity in different conditions: a) Cases 3 and 4 (μ_g = 4.45e–5 kg/ms, ρ_g = 0.311 kg/m^3, ρ_s = 2480 kg/m^3, d_p = 0.15 mm) and b) Cases 26, 27, and 28 (μ_g = 1.79e–5 kg/ms, ρ_g = 1.225 kg/m^3, ρ_s = 2480 kg/m^3, d_p = 0.255 mm).

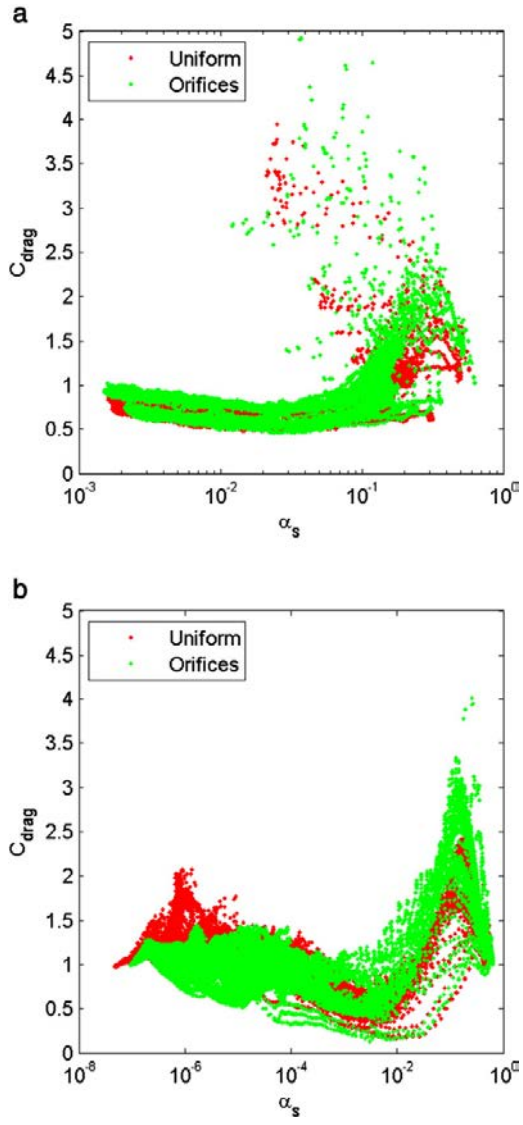

Fig. 15. Effect of orifices in different fluidization conditions: a) CFB Cases 25 and 29 (μ_g = 1.79e–5 kg/ms, ρ_g = 1.225 kg/m^3, ρ_s = 2480 kg/m^3, d_p = 0.255 mm. U_0 = 2.75 m/s), and b) in BFB Cases 23 and 27 (μ_g = 1.79e–5 kg/ms, ρ_g = 1.225 kg/m^3, ρ_s = 2480 kg/m^3, d_p = 0.255 mm. U_0 = 1.25 m/s).

Not only the fluidization velocity but also the way the air is introduced into the riser affects the flow structure. In the previous 2D analysis [7], air distribution was reported to have significant effects on C_{drag} in BFB conditions. Fig. 15 shows the effect of air distribution on C_{drag} in the 3D simulations in CFB and BFB conditions. The geometry in the simulations is a pseudo-2D bed where the orifices are assumed to reach from wall to wall in the depth direction. In CFB conditions the air distribution doesn't show any effect on C_{drag} whereas in BFB conditions C_{drag} increases when the gas flow is divided into separate nozzles. Thus air distributor design should be taken into account in drag modeling. In practice, this can be difficult in which case the possible effects of the air distributor design should be considered in the interpretation of the simulation results as a possible source of inaccuracy.

3.6. Effects of material properties

The previous 2D study [8] showed that the effects of material properties on C_{drag} cannot be described by means of a dimensionless number. Thus the effect of each material property needs to be considered separately. In the previous 2D study of the time-averaged drag force in CFB conditions [8], solid phase density and particle size were found to affect C_{drag}. Both parameters showed a positive effect, i.e. an increase in both particle size or solid material density increased C_{drag}. In BFB conditions [7] the effect of particle size was similar but the effect of density was not positive in all situations. Similar comparison on the basis of the 3D data of this study is presented in Figs. 16 and 17. Fig. 16 shows a positive effect of solid density at low solid concentrations and a negative effect in regions of high solid concentration. The effect of particle size, shown in Fig. 17, is of the same nature but even stronger. However, when reduced particle size leads to a change in the fluidization mode, like in Fig. 17b, the effect of the particle size is complicated, since the highest values of C_{drag} occur in BFBs and CFBs at different ranges of solid volume fractions, as seen in Fig. 17b.

In the earlier 2D studies [7,8], gas phase density was not found to have any significant effect on the drag correction coefficient. However, the range inside which gas density was varied was quite narrow, i.e. the range typically encountered in fluidization with air at atmospheric pressures. At elevated pressures gas density can be significantly higher. Fig. 18 shows a comparison in which gas density was changed while other parameters were kept constant. When the change in gas density is small, i.e. inside the range typical of fluidization at the atmospheric pressure, C_{drag} remains unchanged. At the higher gas density of 6 kg/m^3 in Case 11 shown in Fig. 18, significant effects on C_{drag} occur in the whole range of solid concentrations.

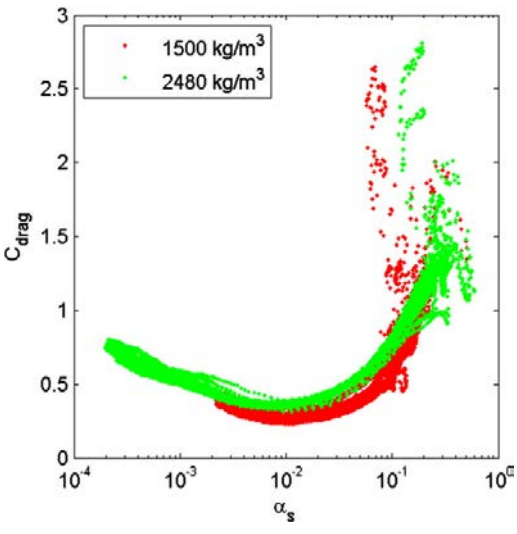

Fig. 16. Effect of solid material density on C_{drag} in different conditions: Cases 14 and 7 (μ_g = 4.45e–5 kg/ms, ρ_g = 1.225 kg/m^3, d_p = 0.255 mm. U_0 = 1.3 m/s).

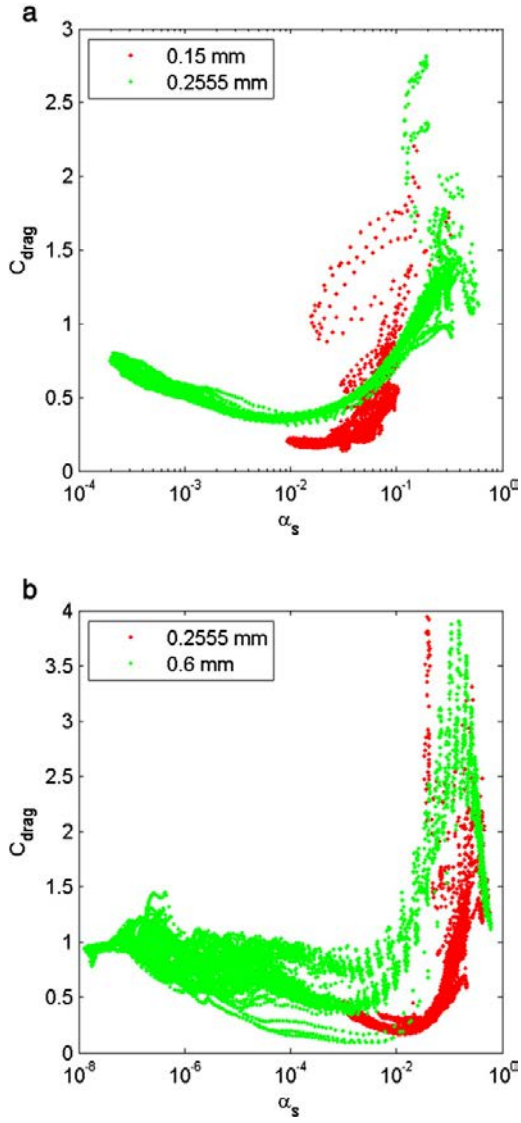

Fig. 17. Effect of particle size on C_{drag} in different conditions: a) Cases 13 and 7 (μ_g = 4.45e–5 kg/ms, ρ_g = 1.255 kg/m^3, ρ_s = 2480 kg/m^3, U_0 = 1.3 m/s), and b) Cases 5 and 2 (μ_g = 4.45e–5 kg/ms, ρ_g = 0.311 kg/m^3, ρ_s = 2480 kg/m^3, U_0 = 2.75 m/s).

The previous 2D studies [7,8] showed that gas viscosity affects C_{drag} negatively. Same qualitative conclusion can be drawn from the 3D results presented in Fig. 19.

4. Conclusions

In the present work, a qualitative analysis of the time-averaged gas–solid drag force in a fluidized bed is carried out. The average drag force is expressed as a product of the drag force calculated from the time-averaged velocities and volume fractions and a correction coefficient.

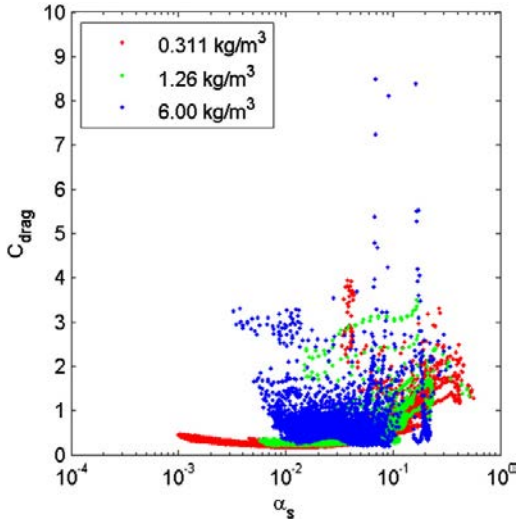

Fig. 18. Effect of gas density on C_{drag} in different conditions: Cases 5, 8 and 11 ($\mu_g = 4.45e{-}5$ kg/ms, $\rho_s = 2480$ kg/m^3, $d_p = 0.255$ mm, $U_0 = 2.75$ m/s).

The analysis is based on a large number of transient 3D simulations of small bubbling, turbulent and circulating fluidized beds. The results are compared with corresponding 2D data and the earlier parametric studies [7,8] carried out on the basis of results from transient 2D CFD simulations. Some of the trends observed in the 2D data are also seen in the 3D analysis, and especially at low solid concentrations, the results are even quantitatively close to each other. In dense regions the results of the present 3D study strongly deviate from the earlier 2D results, which confirms that to accurately model gas–solid drag force in a 3D steady state simulation, the drag model has to be based on data from 3D transient simulations.

To save computational time, most of the simulations in the present work were carried out for a small, pseudo-2D fluidized bed geometry in which the depth of the bed could be described by only three grid points. Comparisons with cases of larger dimensions were also carried out to confirm that the limited geometry didn't significantly affect the conclusions.

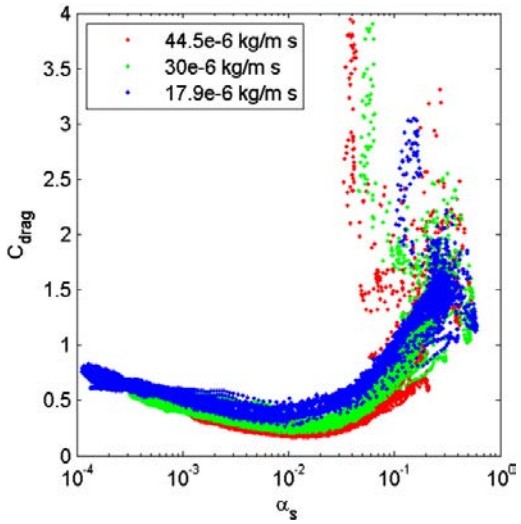

Fig. 19. Effect of gas viscosity on C_{drag} in different condition: Cases 5, 12 and 9 ($\rho_g = 0.311$ kg/m^3, $\rho_s = 2480$ kg/m^3, $d_p = 0.255$ mm, $U_0 = 2.75$ m/s).

The parametric study showed that solid volume fraction, particle size, solid density, gas viscosity, the slip velocity between gas and solids and the lateral distance to a wall have significant effects on the drag correction coefficient. At high gas densities typical of pressurized fluidization even the gas density has a significant effect. A general closure model for the time-averaged drag force in a fluidized bed should be based on these seven variables.

Acknowledgments

The authors gratefully acknowledge the financial support of Tekes, VTT Technical Research Centre of Finland, Etelä-Savon Energia Oy, Fortum, Metso Power Oy and Numerola Oy, and the support from Saarijärven Kaukolämpö Oy (Tekes Dnro 2022/31/2010).

References

[1] Y. Igci, S. Sundaresan, S. Pannala, O'brienT. , R.W. Breault, Coarse-Graining of Two-Fluid Models for Fluidized Gas-Particle Suspensions, 5th Int. Conf. on CFD in the Process Industries, CSIRO, Melbourne, Australia, 2006.
[2] D.Z. Zhang, W.B. VanderHeyden, The effects of mesoscale structures on the macroscopic momentum equations for two-phase flows, Int. J. Multiphase Flow 28 (2002) 805–822.
[3] S. Shah, J. Ritvanen, T. Hyppänen, S. Kallio, Wall effects on space averaged two-fluid model equations for simulations of gas-solid flows in risers, Chem. Eng. Sci. 89 (2013) 206–215.
[4] C.C. Milioli, F.E. Milioli, W. Holloway, K. Agrawal, S. Sundaresan, Filtered two-fluid models of fluidized gas-particle flows: new constitutive equations, 59 (2013) 3265–3275.
[5] V. Taivassalo, S. Kallio, J. Peltola, On time-averaged CFD modeling of circulating fluidized beds, Int. J. Nonlinear Sci. Numer. Simul. 13 (2012) 363–373.
[6] Zh.X. Zeng, L.X. Zhou, A two-scale second-order moment particle turbulence model and simulation of dense gas–particle flows in a riser, Powder Technol. 162 (2006) 27–32.
[7] S. Kallio, J. Peltola, T. Niemi, Modeling of the time-averaged gas–solid drag force in a fluidized bed based on results from transient 2D Eulerian–Eulerian simulations, Powder Technol. 261 (2014) 257–271.
[8] S. Kallio, J. Peltola, T. Niemi, Parametric study of the time-averaged gas–solid drag force in circulating fluidized bed conditions, Powder Technol. 257 (2014) 20–29.
[9] E. Esmaili, N. Mahinpey, Adjustment of drag coefficient correlations in three dimensional CFD simulation of gas–solid bubbling fluidized bed, Adv. Eng. Softw. 42 (2011) 375–386.
[10] T. Li, J. Grace, X. Bi, Study of wall boundary condition in numerical simulations of bubbling fluidized beds, Powder Technol. 203 (2010) 447–457.
[11] ANSYS Inc., ANSYS FLUENT Theory Guide. Release 14.0, Canonsburg, 2011. (2011).
[12] M. Syamlal, W. Rogers, T.J. O'Brien, MFIX Documentation: Volume 1, Theory Guide, National Technical Information Service, Springfield, VA, 1993. (DOE/METC-9411004, NTIS/DE9400087).
[13] C.K.K. Lun, S.B. Savage, D.J. Jeffrey, N. Chepurniy, Kinetic theories for granular flow: inelastic particles in couette flow and slightly inelastic particles in a general flow field, J. Fluid Mech. 140 (1984) 223–256.
[14] D.G. Schaeffer, Instability in the evolution equations describing incompressible granular flow, J. Differ. Equ. 66 (1987) 19–50.
[15] S. Ogawa, A. Umemura, N. Oshima, On the equations of fully fluidized granular materials, J. Appl. Math. Phys. (ZAMP) 31 (1980) 483–493.
[16] D. Gidaspow, Multiphase Flow and Fluidization — Continuum and Kinetic Theory Descriptions, Academic Press, 1994.
[17] S. Ergun, Fluid flow through packed columns, Chem. Eng. Prog. CEP 48 (1952) 89.
[18] C. Wen, Y. Yu, Mechanics of fluidization, Chem. Eng. Prog. Symp. Ser. 62 (1966) 100–111.
[19] S. Kallio, M. Guldén, A. Hermanson, Experimental study and CFD simulation of a 2D circulating fluidized bed, the 20th Int. Conf. on fluidized bed combustion, 2009. (May 18–20, Xi'an, China).
[20] A. Haider, O. Levenspiel, Drag coefficient and terminal velocity of spherical and non-spherical particles, Powder Technol. 58 (1989) 63–70.
[21] W.-C. Yang, Modification and re-interpretation of Geldart's classification of powders, Powder Technol. 171 (2007) 69–74.
[22] T. Niemi, J. Peltola, S. Kallio, Time averaged modeling of BFBs: analysis of the terms in the momentum equations, Proceedings Fluidization XIV Conference, May, Noordwijkerhout, The Netherlands, 2013, pp. 559–566.
[23] T. Li, A. Gel, S. Pennala, M. Shahnam, M. Syamlal, CFD simulations of circulating fluidized bed risers, part i: grid study, Powder Technol. 254 (2014) 170–180.